arXiv:1511.03836v1 [physics.atom-ph] 12 Nov 2015

Collapse and revival of a Dicke-type coherent narrowing in potassium vapor confined in a nanometric-thin cell

A Sargsyan[1], Y Pashayan-Leroy[2], C Leroy[2] and D Sarkisyan[1]

[1]Institute for Physical Research, NAS of Armenia, Ashtarak, Armenia

[2]Laboratoire Interdisciplinaire Carnot de Bourgogne, UMR CNRS 6303, Université de Bourgogne, France

E-mail: davsark@yahoo.com

8, November 2015

Abstract. A nanometer-thin-cell (in the direction of laser beam propagation) has been elaborated with the thickness of the atomic vapor column varying smoothly in the range of $L = 50 - 1500\,\text{nm}$. The cell allows one to study the behavior of the resonance absorption over the D_1 line of potassium atoms by varying the laser intensity and the cell thickness from $L = \lambda/2$ to $L = 2\lambda$ with the step $\lambda/2$ ($\lambda = 770\,\text{nm}$ is the resonant wavelength of the laser). It is shown that despite the huge Doppler broadening ($> 0.9\,\text{GHz}$ at the cell temperature $170\,^\circ\text{C}$), at low laser intensities a narrowing of the resonance absorption spectrum is observed for $L = \lambda/2$ ($\sim 120\,\text{MHz}$ at FWHM) and $L = 3/2\lambda$, whereas for $L = \lambda$ and $L = 2\lambda$ the spectrum broadens. At moderate laser intensities narrowband velocity selective optical pumping (VSOP) resonances appear at $L = \lambda$ and $L = 2\lambda$ with the linewidth close to the natural one. A comparison with saturated absorption spectra obtained in a 1-cm-sized K cell is presented. The developed theoretical model well describes the experiment.

1. Introduction

Several experimental realizations and theoretical predictions concerning thin cells ($5 - 100\,\mu\text{m}$) of atomic vapor have been reported in the literature [1–6]. Recently developed optical nanometer-thin-cell (NTC) containing atomic vapor of alkali metal allows one to observe a number of spectacular phenomena, which are absent in common $0.1 - 10\,\text{cm}$-long cells, particularly: 1) the cooperative Lamb shift caused by dominant contribution of atom-atom interactions [7]; 2) the largest negative group index measured to date $n_g = -10^5$ caused by propagation of near-resonant light through a gas with $L = \lambda/2$ thickness with very high density [8]; 3) strong broadening and shifts of resonances, which become significant when thickness $< 100\,\text{nm}$ caused by atom-surface van der Waals interactions due to the tight confinement in the NTC [9–12].

Below is presented another spectacular phenomenon obtained in the NTC filled with potassium vapor. Earlier it was shown that an important parameter determining

the spectral width, the lineshape and the absorption and fluorescence in these cells is the ratio L/λ with L being the thickness of the vapor column and λ the wavelength of the laser radiation resonant with the atomic transition [13–18]. Particularly, for Rb and Cs atomic vapors it was demonstrated that the spectral linewidth of the resonant absorption reaches its minimum value at the thickness $L = (2n+1)\lambda/2$ (n is an integer); this effect has been termed the Dicke coherent narrowing (DCN). It was shown that for the thickness $L = n\lambda$ the spectral width of the resonant absorption reaches its maximum value close to the Doppler width (of the order of several hundreds of MHz) recorded in common cells of conventional length ($1 - 10\,\mathrm{cm}$). This phenomenon has been termed collapse of DCN (the phenomenon is also absent in common cells) [13–18].

Recently a one-dimensional NTC filled with natural potassium has been constructed. In order to produce K atomic vapor with a density of $\sim 10^{13}\,\mathrm{at/cm^3}$ (it is needed to registrate absorption at the thickness $L = 385\,\mathrm{nm}$) the operation temperature of the NTC's side-arm must be around 150 °C and by 20 °C higher at the NTC windows (to prevent the condensation of K atoms at the NTC windows). For such relatively high temperatures there is a huge Doppler broadening ($> 0.9\,\mathrm{GHz}$). This value is much larger than those of Rb (0.5 GHz) and Cs (0.4 GHz) atomic vapors [19]. Thus, it was not clear beforehand whether DCN and collapse of DCN will be well observable in K vapor. As it is demonstrated below the effect is well observable for potassium vapor, too. It is also shown that the K NTC is a convenient tool for laser spectroscopy.

2. Experiment

2.1. A nano-cell filled with potassium (K) vapor

A one-dimensional nano-metric-thin cell filled with natural potassium (93.3% ^{39}K and 6.7% ^{41}K) has been constructed and used for the experiment. The design of the NTC is similar to that of the extremely thin cell described earlier [20] (the details of NTC design can be found in [7]). The NTC allows one to exploit a variable vapor column thickness L in the range of $50 - 1500\,\mathrm{nm}$. The windows of the NTC are fabricated with well-polished crystalline sapphire with the C-axis perpendicular to the window surface to minimize birefringence. The NTC operates with a specially designed oven with two ports for laser beam transmission.

2.2. Experimental setup

The experimental arrangement is sketched in Fig. 1. The linearly polarized beam of an extended cavity diode laser (with the linewidth $< 1\,\mathrm{MHz}$), resonant with the ^{39}K D_1 line after passing through a Faraday isolator (FI), was focused onto a 0.5 mm diameter spot on the K NTC orthogonally to the cell window. The transmission signal was detected by a photodiode (4) and was recorded by a Tektronix TDS 2014B four-channel storage oscilloscope (5). To record the transmission spectra, the laser radiation was linearly scanned within up to a $\sim 1\,\mathrm{GHz}$ spectral region covering the studied group of

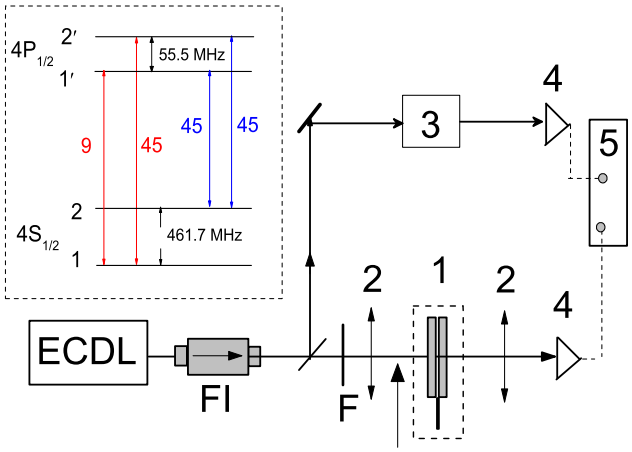

Figure 1. Sketch of the experimental setup. ECDL: diode laser; FI: Faraday isolator; 1 - K NTC with a variable thickness; F-neutral filter, 2 - lenses with a focal length 20 cm: 3 - reference, saturated absorption scheme; 4 - photodetectors; 5 - oscilloscope. The inset shows the energy levels of the ^{39}K D_1 line.

transitions. In order to measure the transmission spectra at different NTC thicknesses, the oven with the NTC was smoothly moved vertically as indicated by an arrow in Fig. 1 (note that although it is technically easier to move only the ETC, in this case the temperature regime of the cell will be changed during the movement). About 30% of the laser power was branched to form the reference spectrum using the saturated absorption (SA) scheme (3) with 1.4-cm long potassium cell [21–24].

2.3. Experimental results

Consider first the two cases with cell thicknesses $L = \lambda/2$ (385 nm) and $L = \lambda$ (770 nm), the most contrasted ones with respect to the length dependence of DCN. Figures 2 and 3 show the transmission spectra (the upper curves) on the ^{39}K D_1 line for a low laser power $P_L = 2\,\mu$W. The first figure shows the spectrum at a cell thickness $L = \lambda/2$, while the second one shows the spectrum for $L = \lambda$. As seen from Fig. 2 there is Dicke-narrowing and all of the four atomic transitions $F = 2, 1 \rightarrow F' = 1, 2$ have sub-Doppler spectral linewidths (~ 120 MHz at FWHM, while the low- and the high-frequency wings of the lineshape extend to a few hundreds of MHz) and are partially resolved. Note, that there is a narrowing by nearly 8 orders of magnitude in the transition linewidths with respect to the Doppler width and the line profile is similar to the profile of time-of-flight broadening [25].

For $L = \lambda/2$, the Dicke-narrowed sub-Doppler absorption profiles simply broaden and saturate in amplitude when increasing the light intensity. Meanwhile for the thickness $L = \lambda$ the spectral width of the resonant absorption spectrum reaches its maximum value (it means the collapse of DCN) close to the Doppler width (of the order of 1 GHz) and there appear sub-Doppler dips of reduced absorption at the line-center on the broad absorption profile (see Fig. 3) with the increase of light intensity.

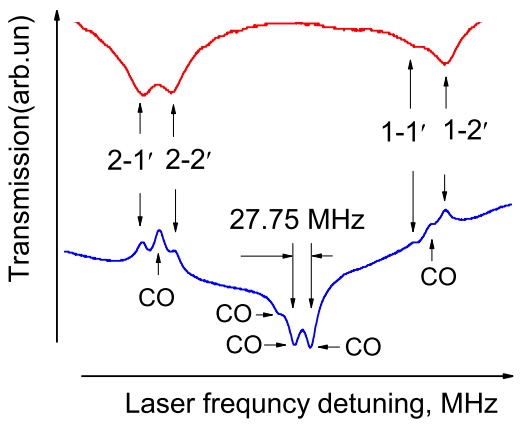

Figure 2. Experimental transmission spectrum (upper curve) of the $F = 2, 1 \rightarrow F' = 1, 2$ transitions on the ^{39}K D_1 line at a cell thickness $L = \lambda/2$ and for a low laser power $P_L = 2\,\mu$W. The lower curve is the SA spectrum. Five cross-over (CO) resonances are marked by the arrows.

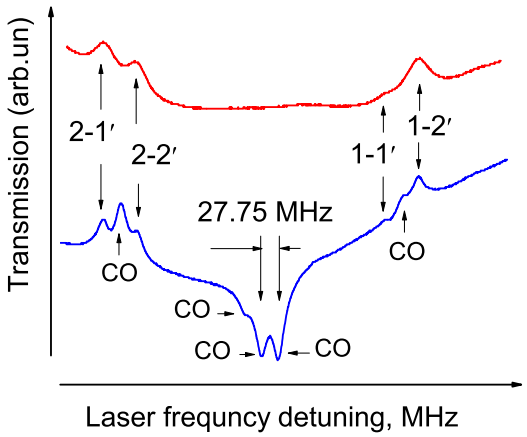

Figure 3. Experimental transmission spectrum (upper curve) of the $F = 2, 1 \rightarrow F' = 1, 2$ transitions on the ^{39}K D_1 line at a cell thickness $L = \lambda$ and for the laser power $P_L = 60\,\mu$W. The lower curve is the SA spectrum. Five cross-over (CO) resonances are marked by the arrows.

These narrowband features resulting from the hyperfine pumping between the two hyperfine components of the ground $4S_{1/2}$ state via the upper excited hyperfine states are called velocity selective optical pumping (VSOP) resonances, that are located at four $F = 1, 2 \rightarrow F' = 1, 2$ transitions. The linewidth of the VSOP could be close to the natural one (~ 6 MHz) [16, 26].

It should be noted, that the use of NTC as the frequency reference for the ^{39}K atomic transitions in comparison with the use of the SA spectra (see Fig. 3) provides several advantages which are as follows : (i) contrary to SA, in the case of NTC, the crossover lines are absent, and this is very important to study the Zeeman spectra; (ii) for the case of NTC where the thickness $L = \lambda$, the ratio of the amplitudes for the VSOP peaks is close to the ratio of the atomic probabilities of the corresponding transitions (for example, as seen from the inset of Fig. 1 the atomic transitions $F = 2 \rightarrow F' = 1$ and $F = 2 \rightarrow F' = 2$ have the same probabilities which is confirmed by the upper curve in Fig. 3), while it is not the case for SA; moreover, as a rule, a strong cycling transition in the SA spectrum has a smaller amplitude in comparison with that of the weaker non-cycling one; (iii) the SA geometry requires counter propagating beams, while a single-beam transmission spectrum is needed for a NTC; and (iv) the laser power needed for spectral reference applications in case of NTC is more than by an order of magnitude less than that needed for SA. The above mentioned advantages demonstrated earlier for the frequency reference based on a Rb NTC [27] are also valid for a K NTC.

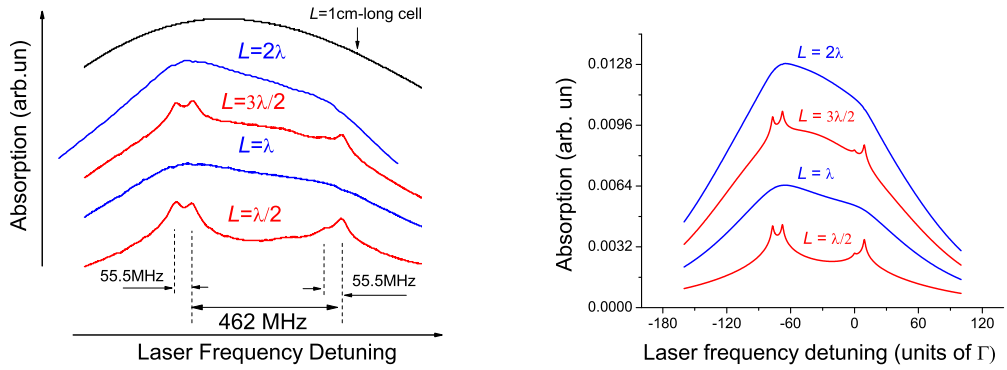

(a) (b)

Figure 4. a) Experimental absorption spectra for the atomic transitions $F = 2, 1 \to F' = 1, 2$ for the low laser power $P_L = 2\,\mu$W at different NTC thicknesses: $L = \lambda/2$, $L = \lambda$, $L = 3\lambda/2$ and $L = 2\lambda$. The side-arm temperature of the NTC is 150 °C. The upper curve shows the absorption in a common 1.4-cm-sized K cell (cell temperature 55 °C). b) Theoretical absorption spectra for a low laser power with the Rabi frequency $\Omega = 0.05$ MHz for different NTC thicknesses: $L = \lambda/2$, λ, $3\lambda/2$ and 2λ.

The experimental absorption spectra for the atomic transitions $F = 2, 1 \to F' = 1, 2$ for the low laser power $P_L = 2\,\mu$W are shown in Fig. 4(a) for different NTC thicknesses varying from $L = \lambda/2$ to $L = 2\lambda$ with the step of $\lambda/2$. As we see for $L = \lambda/2$ and $L = 3\lambda/2$, there is Dicke-narrowing that's why all of the four atomic transitions $F = 1, 2 \to F' = 1, 2$ have sub-Doppler spectral linewidths and are partially resolved (the best spectral resolution is achieved for $L = \lambda/2$). Meanwhile for the thicknesses $L = \lambda$ and 2λ the spectral widths of the resonant absorption spectra reach their maximum values (it means the collapse of the Dicke-narrowing). The theoretical spectra presented in Fig. 4(b) well describe the experiment.

Figure 5(a) shows the experimental absorption spectra at the moderate laser power $P_L = 60\,\mu$W for the cell thickness L varying from $L = \lambda/2$ to $L = 2\lambda$ with the step of $\lambda/2$. As we see for $L = \lambda/2$ and $L = 3\lambda/2$, there is still Dicke-narrowing (while a little spectrally broadened) that's why the atomic transitions $F = 1, 2 \to F' = 1, 2$ are still partially resolved. Meanwhile for the thicknesses $L = \lambda$ and 2λ the spectral widths of the resonant absorption spectra reach their maximum values and there appear small narrowband VSOPs. The calculated absorption spectra (see Fig. 5(b)) well describe the experiment.

The experimental absorption spectra for the high laser power of $P_L = 2.5$ mW for the cell thickness L varying from $L = \lambda/2$ to $L = 2\lambda$ with the step of $\lambda/2$ are shown in Fig. 6(a). As we see for $L = \lambda/2$ and $L = 3\lambda/2$, there is still Dicke-narrowing while spectrally broadened that's why the atomic transitions $F = 1, 2 \to F' = 1, 2$ are worst resolved. Meanwhile for the thicknesses $L = \lambda$ and 2λ the spectral widths of the resonant absorption spectra reach their maximum values and there appear large

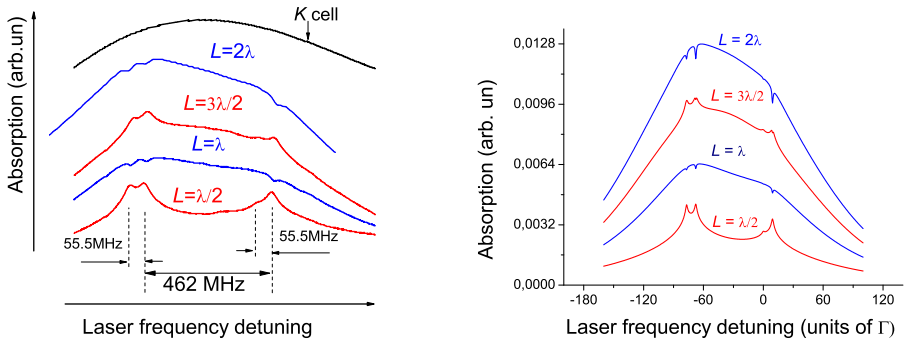

(a) (b)

Figure 5. a) Experimental absorption spectra for the atomic transitions $F = 2, 1 \rightarrow F' = 1, 2$ for a moderate laser power, $P_L = 60\,\mu$W, at different NTC thicknesses: $L = \lambda/2$, λ, $3\lambda/2$ and 2λ. The upper curve shows the absorption of 1.4-cm-long K cell. b) Theoretical absorption spectra for a moderate power with the Rabi frequency of $\Omega = 0.3\,$MHz for different NTC thicknesses: $L = \lambda/2$, λ, $3\lambda/2$ and 2λ.

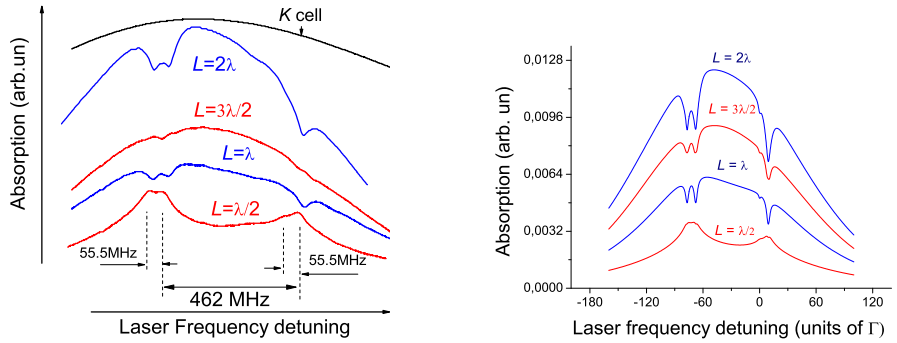

(a) (b)

Figure 6. a) Experimental absorption spectra for the atomic transitions $F = 2, 1 \rightarrow F' = 1, 2$ for a high laser power, $P_L = 2.5\,$mW at different NTC thicknesses: $L = \lambda/2$, λ, $3\lambda/2$ and 2λ. The upper curve shows the absorption of 1.4-cm-long K cell. b) Theoretical absorption spectra for a high laser power with the Rabi frequency of $\Omega = 2\,$MHz for different NTC thicknesses: $L = \lambda/2$, λ, $3\lambda/2$ and 2λ.

narrowband VSOPs. Note that at high laser intensities VSOP resonances appear also for $L = 3/2\lambda$. The theoretical spectra presented in Fig. 6(b) well describe the experiment.

As it was demonstrated earlier for Rb vapor [16] and is confirmed for K vapor (see Figs.4 (a), (b) and Figs. 6(a), 6(b)) the peak absorption at $L = \lambda/2$ is only slightly smaller than that of $L = \lambda$ at low intensities (the absolute value of the peak absorption is $\sim 0.6\%$ for $150\,^{\circ}$C at the side-arm), and the absorption for $L = \lambda/2$ becomes even larger than that of $L = \lambda$ at higher intensities.

With further increasing of the NTC thickness L, the Dicke-narrowed sub-Doppler

absorption profiles simply broaden, their relative contrast decrease and the oscillating character of the Dicke narrowing with the cell thickness vanishes (for Cs vapor the narrowing completely vanishes for $L > 5\,\mu$m [5]). As to the VSOPs as it was demonstrated in [6] they are still observable in Cs vapor at $L \sim 10\,\mu$m (although with a very small amplitude and small signal/noise ratio).

It should be noted, that the presence of the narrow-band resonances at $L = \lambda/2$ (absorption) and $L = \lambda$ (VSOPs) in the NTC filled with ^{39}K allows us to detect complete hyperfine Paschen-Back regime at relatively small magnetic fields [28].

3. Theoretical model

We report here the theoretical model aimed at reproducing the features of absorption spectra registered in the experiment presented in this paper. The model is close to the one described in [29]. We consider a three-level model with the states assigned to the real states of the D_1 line $4S_{1/2} \rightarrow 4P_{1/2}$ of potassium atom (see the inset in Fig. 1). The scheme of the light-atom interaction is presented in Fig. 7. As a ground state $|1\rangle$ we use one of the hyperfine components of the $4S_{1/2}$ ground level ($F = 1$ or $F = 2$) which is coupled to the excited states $|2\rangle$ ($F' = 1$) and $|3\rangle$ ($F' = 2$) by a laser field of amplitude E and frequency ω. The state denoted by $|1'\rangle$ corresponds to the other ground hyperfine component not taken into the model. The electromagnetic field is assumed to be a plane wave propagating through a gas of K atoms confined in a cell of length L along z-direction. Our consideration is conducted within the semiclassical approximation which means the light field is treated classically while the atomic medium is quantized. The detuning of the laser field from the transition $|1\rangle \rightarrow |2\rangle$ is denoted by

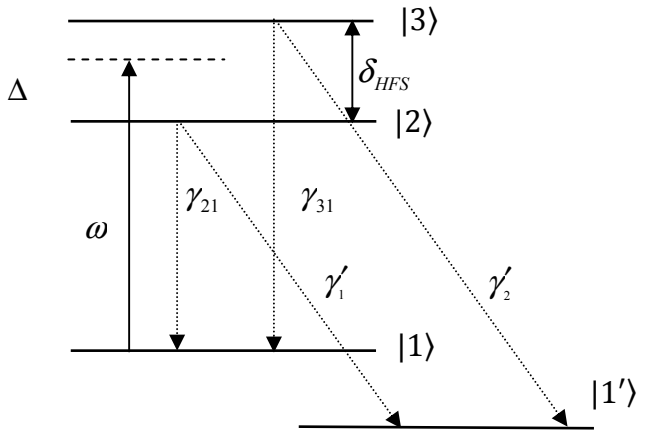

Figure 7. The three-level scheme around the D_1 line of ^{39}K as described in the text.

$\Delta = \omega_{21} - \omega - kv_z$, where kv_z is the Doppler shift contribution for the detuning of the laser field corresponding to the velocity component v_z along the propagation vector $\mathbf{k}$.

The total Hamiltonian in the electric-dipole and rotating-wave approximations

(RWA) [30] for atom-field interacting system can be written as

$$H = H_0 + H_I. \tag{1}$$

H_0 is the unpertubed (i.e. bare) three-state atomic Hamiltonian

$$H_0 = \hbar\Delta|2\rangle\langle 2| + \hbar(\Delta + \delta_{\rm HFS})|3\rangle\langle 3| \tag{2}$$

with $\delta_{\rm HFS}$ being the hyperfine splitting between the upper excited levels, and H_I the atom-field interaction Hamiltonian

$$H_I = -\hbar\Omega_1^*|1\rangle\langle 2| - \hbar\Omega_2^*|1\rangle\langle 3| + h.c. \tag{3}$$

Here $\Omega_{1,2} = d_{1i}E/2\hbar$ are the Rabi frequencies of the corresponding atomic transitions, with d_{1i} $(i = 2, 3)$ being the electric-dipole matrix element associated with the transition $|1\rangle \rightarrow |i\rangle$, and $h.c.$ represents Hermitian conjugate.

We point out the key points of the basic assumptions made in the model: the atomic number density is assumed to be low enough so that the effect of collisions between the atoms can be ignored and only atom-surface collisions are to be considered; the atoms experience inelastic collisions with the cell walls; the incident beam diameters largely exceed the cell thickness so the decoherence due to the diffusion of atoms out of the incident beams is neglected. The effect of the reflection of the radiation from the highly-parallel windows of the nano-cell behaving as a Fabry-Perot cavity [31] is taken into account. The Doppler-broadening effect is included assuming a Maxwellian distribution of velocities.

The internal atomic dynamics is described by a semiclassical density matrix $\rho = \sum \rho_{ij}|i\rangle\langle j|$, the time evolution of which is given by the Liouville equation of motion :

$$\dot{\rho} = -\frac{i}{\hbar}[\hat{H}, \rho] + \Gamma\rho, \tag{4}$$

where Γ is the relaxation operator. The density-matrix equations of motion for a considered three-level system read

$$\begin{aligned}
\rho_{11} &= -2\,\mathrm{Im}(\Omega_1^*\rho_{21}) - 2\,\mathrm{Im}(\Omega_2^*\rho_{31}) + \gamma_{21}\rho_{22} + \gamma_{31}\rho_{33},\\
\rho_{22} &= 2\,\mathrm{Im}(\Omega_1^*\rho_{21}) - 2\Gamma\rho_{22},\\
\rho_{33} &= 2\,\mathrm{Im}(\Omega_2^*\rho_{31}) - 2\Gamma\rho_{33},\\
\rho_{21} &= i\Omega_1(\rho_{11} - \rho_{22}) - i\Omega_2\rho_{32}^* - (\Gamma + i\Delta)\rho_{21},\\
\rho_{31} &= i\Omega_2(\rho_{11} - \rho_{33}) - i\Omega_1\rho_{32} - [\Gamma + i(\Delta + \delta_{HFS})]\,\rho_{31},\\
\rho_{32} &= i\Omega_2\rho_{21}^* - i\Omega_1^*\rho_{31} - (2\Gamma + i\delta_{HFS})\rho_{32},
\end{aligned} \tag{5}$$

and $\rho_{ij} = \rho_{ji}^*$. Here γ_{21} and γ_{31} are the spontaneous decay rates from the excited states $|2\rangle$ and $|3\rangle$ to the ground state $|1\rangle$, $2\Gamma = \gamma_N = \gamma_{21} + \gamma_1' = \gamma_{31} + \gamma_2'$ is the total rate of the spontaneous decay with γ_1', γ_2' being the decay rates describing the optical hyperfine pumping between the two hyperfine components of the ground $4S_{1/2}$ state. For our calculations we take $\gamma_{21} = 1/6\gamma_N$, $\gamma_1' = 5/6\gamma_N$ and $\gamma_{31} = 0.5\gamma_N$, $\gamma_2' = 0.5\gamma_N$, with the natural linewidth $\gamma_N = 2\pi \times 6.03\,\mathrm{MHz}$ for ^{39}K.

We are concerned with the laser field transmitted through the second window of the cell containing the atomic vapor

$$E_{out} = t_2 E_0. \tag{6}$$

Here t_2 is the transmission coefficient of the second window of the cell, and $E_0(z)$ is the laser field inside the cell. The goal is to find an expression for the field $E_0(z)$ at any position z inside the vapour in order to obtain the transmitted signal $I_\propto |E_{out}|^2$. The field can be represented as

$$E_0(z) = E_0'(z) + E_0''(z). \tag{7}$$

Here $E_0'(z)$ is the laser field inside the empty cell, and $E_0''(z)$ is the resonant contribution of the medium to the field. Note that for a very dilute medium $E_0''(z) \ll E_0'(z)$. Under this condition, considering the effects of interference and multiple reflections from the cell windows one obtains for the laser field inside the empty cell [31]

$$E_0'(z) = \mathcal{E} t_1 \frac{1 - r_2 \exp[2ik(L-z)]}{F}, \tag{8}$$

and for the resonant contribution at the cell exit $z = L$ [29]

$$E_0''(z = L) = \frac{2\pi i k}{F} \int_0^{z'=L} \mathcal{P}_0(z') \left[1 - r_1 e^{2ikz'}\right] dz', \tag{9}$$

where $\mathcal{E}$ is the amplitude of the incident laser field and $\mathcal{P}_0(z)$ is the amplitude of the polarization induced inside the vapor at the laser frequency. Here the factor $F = 1 - r_1 r_2 \exp(2ikL)$ takes into account the influence of the beam reflected by the second wall of the cell (which is important in the case where the cell thickness is $L \sim \lambda$), i.e. the Fabry-Perot effect, and r_1 and r_2 are the reflection coefficients of the first and second windows, respectively, and t_1 is the transmission coefficient of the first window. Taking into account the dilute character of the medium ($E_0'' \ll E_0'$), we obtain for the transmitted signal:

$$I \approx t_2^2 \left[|E_0'(L)|^2 + 2\mathrm{Re}\left\{ E_0''(z = L) E_0'^*(z = L) \right\} \right]. \tag{10}$$

The absorption signal of the laser field is given by the second term in the brackets

$$S_{abs} \sim 2\mathrm{Re}\left\{ E_0''(z = L) E_0'^*(z = L) \right\}. \tag{11}$$

To obtain the absorption spectra, we need to calculate the polarization of the medium on the frequency of the laser field that is determined by

$$P_0(z) = N d_{21} \left(\rho_{21}^+ + \rho_{21}^- \right) + N d_{31} \left(\rho_{31}^+ + \rho_{31}^- \right), \tag{12}$$

where nondiagonal matrix elements $\rho_{j1}^+ \equiv \rho_{j1}$ $(z = v_z t)$ and $\rho_{j1}^- \equiv \rho_{j1}$ $(z = L - v_z t)$ with $j = 2, 3$ relate to the atoms flying with the velocity in the positive and negative directions of the cell axis, respectively. We provide this by exact numerical solution of Eqs. (5) by assuming realistic parameters corresponding to the conditions of our modeled experiment. To include the Doppler-broadening effect, we average the density-matrix elements obtained for a single atom over the velocity distribution of the atoms which is considered to be Maxwellian and is given by $W(v) = \frac{N}{u\sqrt{\pi}} \exp[-(\frac{v}{u})^2]$, where v is the

atomic velocity, N is the atomic density, and u is the most probable velocity given by $u = 2k_BT/M$ with k_B being the Boltzmann constant, T the temperature of the vapour in Kelvin and M the atomic mass. Inserting formulas (8), (9), (12) to Eq. (11) one gets for the Doppler broadened absorption profile [29]

$$\frac{1}{\mathcal{E}^2}\langle S_{abs}\rangle = -\frac{4\pi\omega N t_2^2 t_1}{cu\sqrt{u}}\frac{1}{\mathcal{E}|F|^2}\int_0^\infty e^{-v_z^2/u^2}v_z dv_z \int_0^{L/v} dt \\ \times \mathrm{Im}\Big\{\sum_{i=2,3} d_{i1}\Big[\rho_{i1}^+\left(t,\Delta^+,E_0(v_z t)\right)\left(1-r_1 e^{2ikv_z t}\right) \\ + \rho_{i1}^+\left(t,\Delta^-,E_0(L-v_z t)\right)\left(1-r_1 e^{2ik(L-v_z t)}\right)\Big]\Big\}. \tag{13}$$

Here $\Delta^+ = \Delta^+ \pm kv_z$ are the Doppler shifted detunings of the probe field. The plus sign refers to the atoms with the velocity $\mathbf{v}$ in the positive direction of the cell axis, and the minus sign refers to the atoms with the velocity $\mathbf{v}$ in the negative direction of the cell axis.

Figures 4(b)-6(b) present the results for the absorption signal as given by the presented theoretical model. Shown are the absorption spectra versus the laser frequency detuning. To match the theoretical spectra to the relevant experimental ones, a value of the Rabi frequency Ω, was attributed to all the spectra registered at a given intensity I. These values of the Rabi frequency were estimated from $\Omega/2\pi = a\gamma_N\sqrt{I/8}$, where I is the laser intensity in mW/cm^2, $\gamma_N/2\pi$ is the decay rate of the excited state (6.03 MHz), and a is the fit parameter. The fit parameter a was optimized to obtain the best match of theoretical and experimental features, with regard to the whole series of experimental spectra, such as presented in Figs. 4-6 (for our case $a \approx 0.03$). The results of our calculations are in general agreement with those of the experiment.

4. Conclusion

It is demonstrated both experimentally and theoretically that the spectral linewidth of the resonant absorption of potassium ^{39}K vapor contained in a nano-metric thin cell with a variable thickness reaches its minimum value (~ 120 MHz) at the thicknesses $L = \lambda/2$ (385 nm) and $L = 3\lambda/2$ (1155 nm) (despite the huge Doppler broadening of ~ 1 GHz at the cell temperature of $\sim 170\,^\circ$C). The effect is termed the Dicke coherent narrowing, earlier observed for Rb and Cs vapors. For the thicknesses $L = \lambda$ (770 nm) and $L = 2\lambda$ (1540 nm) the spectral width of the resonant absorption reaches its maximum value close to the Doppler width, recorded in common cells of conventional length ($1 - 10$ cm).

For $L = \lambda/2$ and $L = 3\lambda/2$, the Dicke-narrowed sub-Doppler absorption profiles simply broaden and saturate in amplitude when increasing the light intensity. Meanwhile for the thicknesses $L = \lambda$ and 2λ, with the increase in the light intensity there appear narrowband sub-Doppler dips of reduced absorption (VSOPs) at the line-center on the broad absorption profile. Practical applications of the potassium NTC are noted. The calculated theoretical spectra well describe the experiment. A comparison of the

NTC spectra with the well known saturated absorption spectra is provided, and the advantages of the NTC use are shown.

Acknowledgements

The research was conducted in the scope of the International Associated Laboratory IRMAS (CNRS-France & SCS-Armenia).

References

[1] Izmailov A Ch 1992 *Laser Phys.* **2** 762.
[2] Vartanyan T A and Lin D L 1995 *Phys. Rev.* A **51** 1959.
[3] Briaudeau S, Bloch D and Ducloy M 1996 *EPL* **35** 337.
[4] Zambon B, Nienhuis G, 1997 *Opt.Commun.* **143** 308.
[5] Briaudeau S, Saltiel S, Nihenius G, Bloch D and Ducloy M 1998 *Phys. Rev.* A **57** R3169.
[6] Briaudeau S, Bloch D, and Ducloy M 1999 *Phys. Rev.* A **59** 3723.
[7] Keaveney J, Sargsyan A, Krohn U, Sarkisyan D, Hughes I G and Adams C S 2012 *Phys. Rev. Lett.* **108** 173601.
[8] Keaveney J, Hughes I G, Sargsyan A, Sarkisyan D and Adams C S 2012 *Phys. Rev. Lett.* **109** 233001.
[9] Hamdi I *et al* 2005 *Laser Phys.* **15** 987.
[10] Fichet M *et al* 2007 *Europhys. Lett.* **77** 54001.
[11] Whittaker K A, Keaveney J, Hughes I G, Sargsyan A, Sarkisyan D and Adams C S 2014 *Phys. Rev. Lett.* **112** 253201.
[12] Whittaker K A, Keaveney J, Hughes I G, Sargsyan A, Sarkisyan D and Adams C S *Phys. Rev.* A **92** 052706.
[13] Romer RH and Dicke RH 1955 *Phys. Rev.* A **99** 532.
[14] Dutier G, Yarovitski A, Saltiel S, Papoyan A, Sarkisyan D, Bloch D and Ducloy M 2003 *Europhys. Lett.* **63** 35.
[15] Sarkisyan D, Varzhapetyan T, Sarkisyan A, Malakyan Yu, Papoyan A, Lezama A, Bloch D and Ducloy M 2004 *Phys. Rev.* A **69** 065802.
[16] Andreeva C, Cartaleva S, Petrov L, Saltiel S, Sarkisyan D, Varzhapetyan T, Bloch D and Ducloy M 2007 *Phys. Rev.* A **76** 013837.
[17] Cartaleva S, Saltiel S, Sargsyan A, Sarkisyan D, Slavov D, Todorov P, Vaseva K 2009 *J. Opt. Soc. Am.* B **26** 1999.
[18] Varzhapetyan T, Nersisyan A, Babushkin V, Sarkisyan D, Vdović S, Pichler G 2008. *J. Phys. B: At. Mol. Opt. Phys.* **41** 185004
[19] Demtroder W 2002 *Laser Spectroscopy: Basic Concepts and Instrumentation* (Springer).
[20] Sarkisyan D, Bloch D, Papoyan A, and Ducloy M 2001 *Opt. Commun.* **200** 201.
[21] Bloch D, Ducloy M, Senkov N, Velichansky V and Yudin V 1996 *Laser Phys.* **6** 670.
[22] Pahwa K, Mudarikwa L, Goldwin J 2012 *Opt. Express* **20** 17456.
[23] Hanley R K, Gregory P D, Hughes I G, Cornish S L 2015 *J. Phys. B: At. Mol. Opt. Phys.* **48** 195004.
[24] Zentile M A, Keaveney J, Weller L, Whiting D J, Adams C S, Hughes I G 2015 *Comput. Phys. Commun.* **189** 162.
[25] Meschede Dieter 2007 *Optics, Light and Lasers* (Wiley-VCH Verlag GmbH and Co., ISBN 978-3-527-40628-9) p 404
[26] Dey S, Ray B, Ghosh P N, Cartaleva S, Slavov D 2015 *Opt. Commun.* **356** 378
[27] Sargsyan A, Sarkisyan D, Papoyan A, Pashayan-Leroy Y, Moroshkin P, Weis A, Khanbekyan A, Mariotti E, Moi L 2008 *Laser Phys.* **18** 749

[28] Sargsyan A, Tonoyan A, Hakhumyan G, Leroy C, Pashayan-Leroy Y, Sarkisyan D 2015 *EPL* **110** 23001
[29] Nikogosyan G, Sarkisyan D, and Malakyan Yu 2004 *J. Opt. Technol.* **71**, 602607.
[30] Shore BW 1990 *The Theory of Coherent Atomic Excitation* (Wiley, New York).
[31] Dutier G, Saltiel S, Bloch D, and Ducloy M 2003 *JOSA* B **20**, 793800.